Hierarchical $Cu_4V_{2.15}O_{9.38}$ micro-/nanostructures: a lithium intercalating electrode material†

Liang Zhou,[a] Wangjun Cui,[a] Jiamin Wu,[a] Qingfei Zhao,[b] Hexing Li,[b] Yongyao Xia,[a] Yunhua Wang[a] and Chengzhong Yu*[ac]

Received 7th September 2010, Accepted 5th November 2010
DOI: 10.1039/c0nr00657b

Hierarchical $Cu_4V_{2.15}O_{9.38}$ micro-/nanostructures have been prepared by a facile "forced hydrolysis" method, from an aqueous peroxovanadate and cupric nitrate solution in the presence of urea. The hierarchical architectures with diameters of 10–20 μm are assembled from flexible nanosheets and rigid nanoplates with widths of 2–4 μm and lengths of 5–10 μm in a radiative way. The preliminary electrochemical properties of $Cu_4V_{2.15}O_{9.38}$ have been investigated for the first time and correlated with its structure. This material delivers a large discharge capacity of 471 mA h g^{-1} above 1.5 V, thus making it an interesting electrode material for primary lithium ion batteries used in implantable cardioverter defibrillators.

Introduction

Primary and secondary batteries, which provide back-up for intermittent wind and solar energy and thus represent one of the most important energy storage and conversion devices nowadays, are playing more and more important roles in modern society.[1–11] They are currently being developed to power an increasingly diverse range of applications, from microchips to cars. One significant role that the batteries play in biomedical area is to power implantable cardioverter defibrillators (ICDs), which are widely applied to hundreds of millions of cardiovascular patients.[12–15] The cardiovascular disease was the number one cause of death and caused an estimated 17.5 million people deaths in 2005, representing 30% of the global deaths according to the World Health Organization.[16] The ICDs, which are powered by primary lithium ion batteries, continuously monitor the heartbeats; when dangerous arrhythmias are detected, they deliver one or more high-energy electric shocks to return the heart to a normal rhythm; thus, they can effectively protect the cardiovascular patients against sudden cardiac death.[12]

Lithium/silver vanadium oxide (SVO) is the dominating type of cathode currently used in primary batteries for ICDs owing to its high energy density, high power performance and long-term stability.[12,15,17,18] However, from the standpoint of future applications, the batteries for ICDs are facing more stringent requirements, including larger discharge capacity, higher power capability, and longer lifespan.[12,19] Since the performances of lithium ion batteries are mainly cathode limited,[20] the seeking of alternative cathode materials for ICDs with improved performance is of significant scientific and technological importance. Recent studies on hybrid $Ag_2V_4O_{11}$-CF_x,[21] $Ag_4V_2O_6F_2$,[22–24] SVO nanowires,[18,25] silver molybdenum oxyfluorides,[26,27] silver vanadium phosphorus oxides,[28–30] silver iron vanadates,[31] CuV_2O_6 micro-/nanostructures[19] have shown exciting enhancement over discharge capacity, high rate capability, discharge voltage, or cycling performance.

Among the potential candidates, copper vanadium oxides (CVOs, also called copper vanadates) are of particular interest. The benefits of CVOs over SVO include not only the much lighter atomic weight and much lower cost of Cu when compared with Ag, but also the fact that Cu^{2+} takes a two-electron reduction process to Cu^0 during the discharge rather than the single-electron reduction.[19] Thus, it is reasonable to expect that CVOs may deliver higher energy density than that of SVO by taking advantage of the two-electron Cu^{2+}/Cu redox couple. Indeed, according to a recent report by Ma *et al.*,[19] α-CuV_2O_6 mesowires and nanowires may deliver a discharge capacity as high as 447–514 mA h g^{-1}, much larger than that of SVO which has a capacity of 315 mA h g^{-1}. Moreover, CVOs have a wide variety of crystalline phases,[19,32–37] such as CuV_2O_6, $Cu_{2.33}V_4O_{11}$, ε-$Cu_{0.85}V_2O_5$, $Cu_2V_2O_7$, $Cu_5V_2O_{10}$, $Cu_{1.1}V_4O_{11}$, $Cu_{11}V_6O_{26}$, and $Cu_4V_{2.15}O_{9.38}$. Although most of the CVO phases have been demonstrated to be potential cathode materials for either primary or secondary lithium ion batteries, the electrochemical properties of $Cu_4V_{2.15}O_{9.38}$ have been ignored since its discovery.[32] Therefore, it is of interest to investigate the electrochemical performance of this compound.

Here we report the synthesis of hierarchical $Cu_4V_{2.15}O_{9.38}$ micro-/nanostructures *via* a facile "forced hydrolysis" method. The superstructures are assembled from flexible nanosheets and rigid nanoplates in a radiative way. The hierarchical micro-/nanostructures provide this material with a large discharge capacity of 471 mA h g^{-1} at 5 mA g^{-1} (above 1.5 V), thus making

[a]*Department of Chemistry and Shanghai Key Laboratory of Molecular Catalysis and Innovative Materials, Fudan University, Shanghai, 200433, P.R. China*
[b]*Department of Chemistry, Shanghai Normal University, Shanghai, 200234, P.R. China*
[c]*ARC Centre of Excellence for Functional Nanomaterials and Australian Institute for Bioengineering and Nanotechnology, The University of Queensland, Brisbane, QLD, 4072, Australia. E-mail: c.yu@uq.edu.au; Fax: +61-7-334 63973; Tel: +61-7-334 63283*

† Electronic supplementary information (ESI) available: SEM images of hierarchical $Cu_4V_{2.15}O_{9.38}$, CV curves of the electrode and discharge profiles of the cell made from $Cu_4V_{2.15}O_{9.38}$ hierarchical structures, XRD pattern and SEM images of layered vanadium oxide hydrate, structure model of $Cu_4V_{2.15}O_{9.38}$. See DOI: 10.1039/c0nr00657b

it an interesting candidate for primary lithium ion batteries used in ICDs.

Experimental section

Synthesis

In a typical synthesis, 5.0 mmol of vanadium pentoxide (V_2O_5) was dissolved in 100 mL of 3.0 wt% hydrogen peroxide (H_2O_2) solution at 25 °C to form a orange-colored clear solution. After stirring for 12 h at this temperature, 15 mmol (0.90 g) of urea ($CO(NH_2)_2$) and 5 mmol (1.2 g) of cupric nitrate trihydrate ($Cu(NO_3)_2 \cdot 3H_2O$) were added to the above solution. The mixture solution was sealed in a Teflon-lined autoclave and hydrothermally treated at 200 °C for 24 h. The products were collected by filtration, washed with water thoroughly for 3 times, and dried at room temperature.

Characterization

X-Ray diffraction (XRD) pattern was recorded on a Bruker D4 X-Ray Diffractometer with Ni-filtered Cu Kα radiation at a voltage of 40 kV and a current of 40 mA. Scanning electron microscopy (SEM) images were obtained on a Philips XL30 microscope operated at 20 kV. Transmission electron microscope (TEM) experiments were conducted on a JEOL 2100 microscope with an accelerating voltage of 200 kV.

Electrochemical measurement

The electrochemical test was characterized in a CR2016-type coin cell. The working electrodes were prepared by mixing 80% active material (namely the as-prepared $Cu_4V_{2.15}O_{9.38}$), 10% carbon black, and 10% polyvinylidene fluoride (PVDF) dissolved in *N*-methylpyrrolidinone (NMP). The slurries of the mixture were coated on stainless steel foil. After coating, the electrodes were dried at 80 °C for 10 min to remove the solvent before pressing. The electrodes were cut into sheets with 1 cm^2 in area, vacuum-dried at 100 °C for 24 h, and weighed before assembly. The weight of active material on each electrode was ~8 mg. The cell assembly was operated in a glove box (model 100G, MBraun, Germany) filled with pure argon. The electrolyte solution was 1 M $LiPF_6$ in ethylene carbonate (EC)/diethyl carbonate (DMC)/ethyl methyl carbonate (EMC) (1 : 1 : 1 by volume). The cells were assembled with the cathode as-prepared, lithium metal as an anode, and Celgard 2300 film as a separator. The capacity of the electrode was measured by a galvanostatic discharge method at 5–80 mA g^{-1} to the cutoff voltage of 1.5 V, using a LAND CT2001A Battery Cycler (Wuhan, China) at room temperature. The capacity (above 1.5 V) was calculated based on the amount of the active material, excluding the weight of the additives in the electrode. The cyclic voltammogram (CV) was performed on a CHI660 electrochemical workstation (CHI, USA) at a scanning rate of 0.1 mV s^{-1} and at room temperature.

Results

The $Cu_4V_{2.15}O_{9.38}$ hierarchical micro-/nanostructures were prepared by a "forced hydrolysis" method from an aqueous peroxovanadate and cupric nitrate solution in the presence of urea. Fig. 1 shows the XRD pattern of the as-synthesized $Cu_4V_{2.15}O_{9.38}$ hierarchical structures. All the diffraction peaks can be indexed to orthorhombic $Cu_4V_{2.15}O_{9.38}$ with the lattice parameters of $a = 1.502$ nm, $b = 0.8564$ nm, $c = 0.6055$ nm and a space group of $P2_12_12_1$ (Joint Committee on Powder Diffraction Standards, JCPDS Card No. 70-1696). No other peaks have been detected, suggesting the high purity of the sample. The relatively broad diffraction peaks demonstrate the nanocrystalline characteristic of the $Cu_4V_{2.15}O_{9.38}$ products.

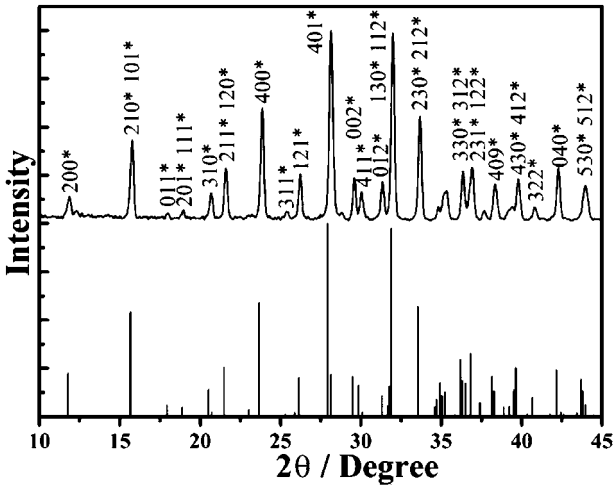

Fig. 1 XRD pattern of the as-synthesized $Cu_4V_{2.15}O_{9.38}$ hierarchical structures.

Fig. 2 and S1† represent the SEM images of the as-synthesized $Cu_4V_{2.15}O_{9.38}$ products. Large quantities of $Cu_4V_{2.15}O_{9.38}$ hierarchical architectures with diameters of 10–20 μm and high purity can be observed in Fig. S1†. As can be seen from higher magnification SEM images (Fig. 2), the superstructures are assembled from thin and flexible nanosheets (indicated by black arrows) and relatively thick and rigid nanoplates (indicated by white arrows) in a radiative way. The nanosheets and nanoplates have similar lengths (5–10 μm) and widths (2–4 μm). Both the nanosheets and the nanoplates have sharp tips and smooth surfaces.

To understand the detailed structural and morphological characteristics of the as-synthesized products, TEM technology was employed. A typical TEM image of a well-developed single $Cu_4V_{2.15}O_{9.38}$ nanosheet broken from the superstructures by ultrasonication is shown in Fig. 3a. Instead of being perfectly flat, the nanosheet displays some intrinsic out-of-plane wrinkles which indicate the high crystallinity and the ultrathin nature of the nanosheet. The corresponding selected area electron diffraction (SAED) pattern, as shown in Fig. 3b, shows a set of diffraction spots which indicate the single-crystalline characteristic of the nanosheet, and it can be indexed to the [100] zone axis of orthorhombic $Cu_4V_{2.15}O_{9.38}$. What's worth mentioning is that, besides the strong diffraction spots such as 020* and 002*, some weak diffraction spots can also be found at those forbidden sites (such as 010* and 001*) as indicated by white arrows in Fig. 3b. A possible reason for those weak spots is the high-order Laue zone caused by the combination of ultrathin nature of the nanosheet (elongation of the spots along the normal of the nanosheet) and the large {100} spacing (narrowed Laue zones

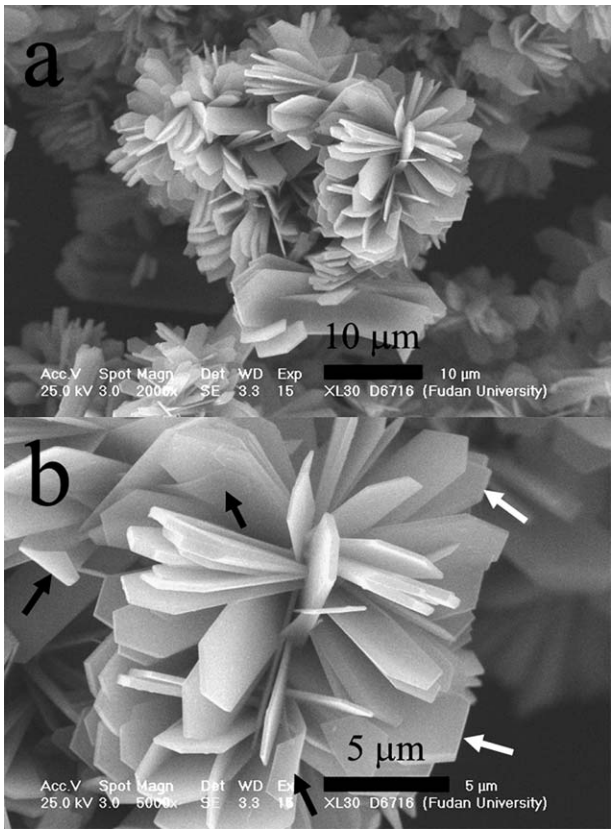

Fig. 2 SEM images of the as-synthesized $Cu_4V_{2.15}O_{9.38}$ hierarchical structures.

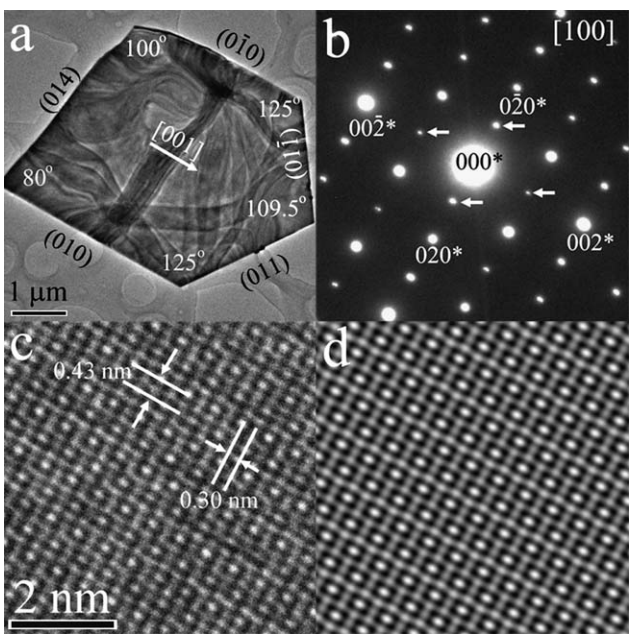

Fig. 3 TEM image (a), ED pattern (b), HRTEM (c) and simulated HRTEM images (d) of a single $Cu_4V_{2.15}O_{9.38}$ nanosheet.

along [100] direction). Similar phenomenon has also been found in the case of $WO_3 \cdot 0.33H_2O$ nanosheets in our previous study.[38] A combination of the TEM and the corresponding ED pattern suggests that the nanosheet grows along the [001] direction, and the top and bottom surfaces are {100} planes, while the other surfaces of the nanosheet are surrounded by the {014}, {010} and {011} planes. The high resolution TEM (HRTEM) image of the nanosheet and the corresponding simulated one are shown in Fig. 3c and d, respectively. Two sets of atomic spacings can be distinguished from Fig. 3c clearly, which correspond to the {020} (0.43 nm) and {002} (0.30 nm) lattice fringes.

A typical TEM image of an individual nanoplate and the corresponding SAED pattern are shown in Fig. 4a and b, respectively. The diffraction spots shown in Fig. 4b indicate the single-crystalline nature of the nanoplate, which can be indexed to the [120] zone. Again, besides the allowed diffraction spots, some forbidden spots can also be observed in Fig. 4b such as 001* and 00$\bar{1}$* as indicated by white arrows. However, in this case (relatively thick nanoplate), the unusual 001* and 00$\bar{1}$* spots are due to double diffraction caused by the dynamic scattering of the strong electron beam rather than "high-order Laue zone" in the nanosheet case. By comparing Fig. 4a and b, it is confirmed that the nanoplate also grows along the [001] direction, the top and bottom surfaces of the nanoplate are {120} planes, and the other surfaces are enclosed by the {210} and {211} planes. Fig. 4c and d represent the HRTEM image and the simulated HRTEM image of the nanoplate, respectively. The {002} (0.30 nm) and {210} (0.56 nm) spacings can be observed clearly from Fig. 4c.

From Fig. 3 and 4, it has been confirmed that both the nanosheets and nanoplates grow along the [001] direction; however, they may have different normals, *i.e.* [100] or [120]. It should be mentioned that not all the nanoplates have a normal of [120] direction, and *vice versa*. However, one can distinguish the normals by measuring the angle of the tips of the nanosheets or nanoplates, since the dihedral angle between the (011) and (01$\bar{1}$) planes is 70.5° (or 180° − 70.5° = 109.5°, see Fig. 3a), and the dihedral angle between the (2$\bar{1}$1) and ($\bar{2}$11) planes is 94° (or 180° − 94° = 86°, see Fig. 4a).

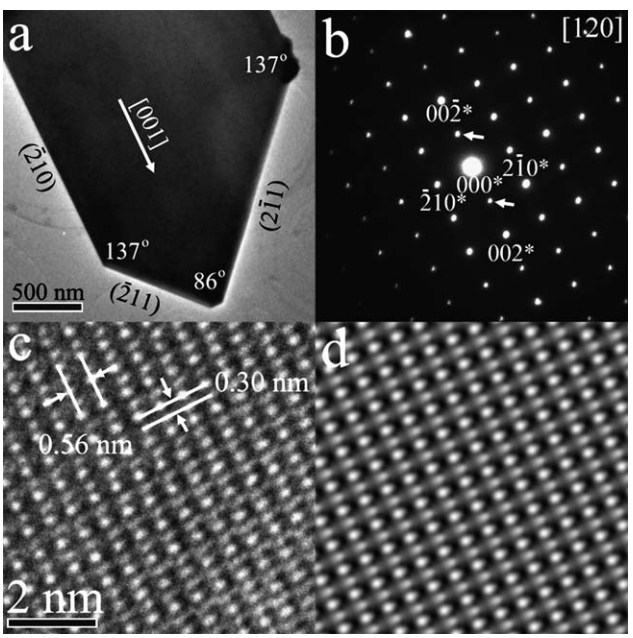

Fig. 4 TEM image (a), ED pattern (b), HRTEM (c) and simulated HRTEM images (d) of a single $Cu_4V_{2.15}O_{9.38}$ nanoplate.

The preliminary electrochemical properties of the as-prepared hierarchical $Cu_4V_{2.15}O_{9.38}$ micro-/nanostructures have also been studied. Fig. S2† shows the cyclic voltammogram (CV) of the electrode made from the as-synthesized $Cu_4V_{2.15}O_{9.38}$ product for the first cycle at a scan rate of 0.1 mV s^{-1} in the potential window of 3.0–1.0 V. In the cathodic polarization process, a strong peak at ~1.9 V *vs.* Li^+/Li can be observed. Since $Cu_4V_{2.15}O_{9.38}$ is composed of V^{5+} and Cu^{2+}, this peak can be assigned to the reduction of V^{5+} and Cu^{2+} due to the lithium intercalation. During the following anodic polarization, no peaks can be observed, which means the lithium intercalation process is irreversible. Similar irreversible lithium insertion behavior has also been reported in Ma *et al.*'s[19] study on α-CuV_2O_6 nano/mesowires.

Fig. 5 displays the discharge profiles of the electrode made from as-prepared $Cu_4V_{2.15}O_{9.38}$ micro-/nanostructures between 3.0 and 1.5 V at various current densities. At a current density of 5 mA g^{-1}, a flat plateau at ~2.2 V can be identified in the first discharge profile. The initial discharge capacity of the as-synthesized $Cu_4V_{2.15}O_{9.38}$ product to a cutoff voltage of 1.5 V is 471 mA h g^{-1}, which is equivalent to an intercalation of approximately 9 Li^+ per formula unit according to the Faraday equation. By increasing the current density from 5 mA g^{-1} to 80 mA g^{-1}, both the discharge voltage plateau and discharge capacity drop slightly. At a current density of 80 mA g^{-1}, the capacity retains 348 mA h g^{-1}, 74% of that under 5 mA g^{-1}. In agreement with the CV results (irreversible lithium insertion behavior), the capacity fades rapidly during the following cycles (Fig. S3†).

Discussion

The utilization of urea in the "forced hydrolysis"[39–42] plays an essential role in the successful preparation of $Cu_4V_{2.15}O_{9.38}$ phase. It has been reported that a direct hydrothermal treatment of a peroxovanadate solution leads to the formation of single crystalline V_2O_5 nanobelts *via* a layered vanadium oxide hydrate ($V_2O_5 \cdot nH_2O$) intermediate phase.[43] In order to investigate the effects of urea, a controlled experiment (the synthesis conditions were identical with those of hierarchical $Cu_4V_{2.15}O_{9.38}$ in this case except no urea was used) was performed. When cupric nitrate trihydrate was introduced into the aqueous peroxovanadate solution and hydrothermally treated at 200 °C for 24 h, rather than the $Cu_4V_{2.15}O_{9.38}$ phase, layered vanadium oxide hydrate phase[43–45] was obtained as confirmed by XRD and SEM characterizations (Fig. S4 and S5†, respectively). The basal distance deduced from the position of the first diffraction peak, $d = 1.36$ nm, is a little smaller than that reported by Li *et al.*[43] (1.42 nm), while larger than that shown by Alonso and Livage[45] (1.2 nm). Only when urea (10–20 mmol) is introduced simultaneously with cupric nitrate trihydrate, hierarchical $Cu_4V_{2.15}O_{9.38}$ micro-/nanostructures can be obtained (Fig. 1).

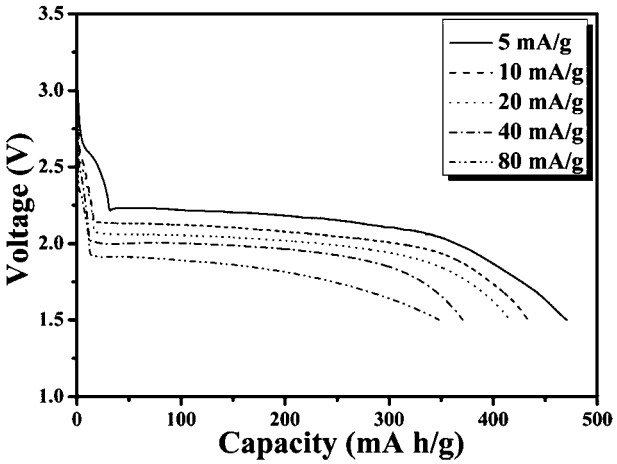

Fig. 5 Discharge profiles of the cell made from $Cu_4V_{2.15}O_{9.38}$ micro-/nanostructures at various current densities of 5–80 mA g^{-1} between 3.0 and 1.5 V.

It is well-known that vanadium forms a wide variety of polyanions under different pH conditions.[46,47] In our system, the pH value of the solution is controlled *in situ* by the hydrolysis of urea. Thus, the dosage of urea also affects the formation of vanadium species. It is therefore not surprising that the Cu/V ratio in the products (4/2.15) differs significantly from the initial Cu/V ratio (1/2) in the solution since not all of the vanadium species precipitate in the reaction. In other words, some vanadium may exist in the solution after reaction in the form of polyanions. Considering that the final pH value of the supernatant after hydrothermal treatment is between 8.5 and 9.0, most of the vanadium may exist in the forms of $VO_3OH_2^-$, $V_4O_{12}^{4-}$ and $V_3O_9^{3-}$ in the solution.[46,47] Similar phenomenon has also been observed in the synthesis of β-$AgVO_3$ as reported by Song *et al.*[48]

With regard to CVOs, some phases can electrochemically react with Li^+ reversibly, thus can be fabricated into secondary batteries;[35,36,49,50] while others cannot, and they can only be used in primary batteries.[19] As we mentioned above, the electrochemical reaction between $Cu_4V_{2.15}O_{9.38}$ and Li^+ is irreversible. Two major reasons account for this irreversibility. First, as shown in the structure of $Cu_4V_{2.15}O_{9.38}$ in Fig. S6†, a majority of the vanadium atoms sit in [VO_4] tetrahedral, and the other vanadium atoms sit in [VO_5] trigonal bipyramids, while after the V^{5+}/V^{4+} reduction process, the V^{4+} ions are not stable in a tetrahedral environment.[22,35] Second, due to the intrinsic large Cu/V ratio of $Cu_4V_{2.15}O_{9.38}$, the [VO_x] polyhedrals cannot maintain the original and relatively rigid structure after the Cu^{2+}/Cu^0 reduction process. Thus, this Cu rich $Cu_4V_{2.15}O_{9.38}$ phase can only find applications in primary lithium ion batteries.

Based on the formula $Cu_4V_{2.15}O_{9.38}$, and assuming the complete reduction of Cu^{2+} to Cu and V^{5+} to V^{3+}, it may be expected that up to 12.3 Li^+ can be accommodated by this material. This would result in a capacity of 644 mA h g^{-1}. If the reduction of Cu^{2+} to Cu is only followed by the reduction of V^{5+} to V^{4+}, the theoretical capacity would be 531 mA h g^{-1}. A practical capacity of 471 mA h g^{-1} has been achieved in the current study. When compared $Cu_4V_{2.15}O_{9.38}$ to the commercial SVO cathode ($Ag_2V_4O_{11}$) for ICDs, the former has a much larger theoretical and practical capacity over 1.5 V, but lower discharge potential. For $Cu_4V_{2.15}O_{9.38}$, the discharge plateau is at ~2.2 V; while for $Ag_2V_4O_{11}$, there are two plateaus, an initial one at ~3.25 V, and a secondary one at roughly 2.5 V. The extended capacity of $Cu_4V_{2.15}O_{9.38}$ can be attributed to the two-electron reduction of Cu^{2+} and the lighter atomic weight of Cu compared to that of Ag. The lower potential is arisen from the lower redox potential of Cu^{2+}/Cu (0.34 V *vs.* NHE) compared to that of

Ag^+/Ag (0.80 V *vs.* NHE). Considering the relatively low discharge voltage of this material, further improvement of the discharge potential by methods such as fluoride incorporation[22] is required.

Conclusions

In summary, we have successfully prepared hierarchical $Cu_4V_{2.15}O_{9.38}$ micro-/nanostructures *via* a facile "forced hydrolysis" method. Preliminary electrochemical characterization demonstrates that this material delivers a much larger discharge capacity (471 mA h g^{-1} above 1.5 V), but lower discharge potential than that of commercial SVO cathode for ICDs. Our contribution provides insights for the synthesis of novel electrode materials with extended capacity. Nevertheless, the $Cu_4V_{2.15}O_{9.38}$ material in the current study cannot fulfil all the requirements for ICD cathodes, further improvement of the discharge voltage of this material should be carried out by methods such as fluoride incorporation.[22]

Acknowledgements

The authors thank Prof. Jin Zou for helpful discussions. This work is supported by the 973 Program (2010CB226901), Science & Technology Commission of Shanghai Municipality (0852nm01500) and SLADP (B108, B113).

References

1 J. M. Tarascon and M. Armand, *Nature*, 2001, **414**, 359.
2 M. S. Whittingham, *Chem. Rev.*, 2004, **104**, 4271.
3 A. S. Arico, P. Bruce, B. Scrosati, J. M. Tarascon and W. Van Schalkwijk, *Nat. Mater.*, 2005, **4**, 366.
4 M. Armand and J. M. Tarascon, *Nature*, 2008, **451**, 652.
5 J. Chen and F. Y. Cheng, *Acc. Chem. Res.*, 2009, **42**, 713.
6 F. Cheng, Z. Tao, J. Liang and J. Chen, *Chem. Mater.*, 2008, **20**, 667.
7 Y. G. Guo, J. S. Hu and L. J. Wan, *Adv. Mater.*, 2008, **20**, 2878.
8 Y. Wang and G. Z. Cao, *Adv. Mater.*, 2008, **20**, 2251.
9 P. G. Bruce, B. Scrosati and J. M. Tarascon, *Angew. Chem., Int. Ed.*, 2008, **47**, 2930.
10 J. B. Goodenough and Y. Kim, *Chem. Mater.*, 2010, **22**, 587.
11 J. M. Tarascon, N. Recham, M. Armand, J. N. Chotard, P. Barpanda, W. Walker and L. Dupont, *Chem. Mater.*, 2010, **22**, 724.
12 A. M. Crespi, S. K. Somdahl, C. L. Schmidt and P. M. Skarstad, *J. Power Sources*, 2001, **96**, 33.
13 J. Drews, G. Fehrmann, R. Staub and R. Wolf, *J. Power Sources*, 2001, **97–98**, 747.
14 P. M. Skarstad, *J. Power Sources*, 2004, **136**, 263.
15 K. J. Takeuchi, A. C. Marschilok, S. M. Davis, R. A. Leising and E. S. Takeuchi, *Coord. Chem. Rev.*, 2001, **219**, 283.
16 *Cardiovascular disease home from Word Health Organization (WHO)*, http://www.who.int/cardiovascular_diseases/en/.
17 Q. L. Bao, S. J. Bao, C. M. Li, X. Qi, C. T. Pan, J. F. Zang, W. L. Wang and D. Y. Tang, *Chem. Mater.*, 2007, **19**, 5965.
18 S. Y. Zhang, W. Y. Li, C. S. Li and J. Chen, *J. Phys. Chem. B*, 2006, **110**, 24855.
19 H. Ma, S. Y. Zhang, W. Q. Ji, Z. L. Tao and J. Chen, *J. Am. Chem. Soc.*, 2008, **130**, 5361.
20 J. Thomas, *Nat. Mater.*, 2003, **2**, 705.
21 K. Chen, D. R. Merritt, W. G. Howard, C. L. Schmidt and P. A. Skarstad, *J. Power Sources*, 2006, **162**, 837.
22 E. M. Sorensen, H. K. Izumi, J. T. Vaughey, C. L. Stern and K. R. Poeppelmeier, *J. Am. Chem. Soc.*, 2005, **127**, 6347.
23 T. A. Albrecht, F. Sauvage, V. Bodenez, J. M. Tarascon and K. R. Poeppelmeier, *Chem. Mater.*, 2009, **21**, 3017.
24 F. Sauvage, V. Bodenez, H. Vezin, T. A. Albrecht, J. M. Tarascon and K. R. Poeppelmeier, *Inorg. Chem.*, 2008, **47**, 8464.
25 F. Sauvage, V. Bodenez, J. M. Tarascon and K. R. Poeppelmeier, *J. Am. Chem. Soc.*, 2010, **132**, 6778.
26 W. Tong, W. S. Yoon, N. M. Hagh and G. G. Amatucci, *Chem. Mater.*, 2009, **21**, 2139.
27 F. Sauvage, V. Bodenez, J. M. Tarascon and K. R. Poeppelmeier, *Inorg. Chem.*, 2010, **49**, 6461.
28 A. C. Marschilok, K. J. Takeuchi and E. S. Takeuchi, *Electrochem. Solid-State Lett.*, 2009, **12**, A5.
29 E. S. Takeuchi, A. C. Marschilok, K. Tanzil, E. S. Kozarsky, S. Zhu and K. J. Takeuchi, *Chem. Mater.*, 2009, **21**, 4934.
30 A. C. Marschilok, E. S. Kozarsky, K. Tanzil, S. Zhu, K. J. Takeuchi and E. S. Takeuchi, *J. Power Sources*, 2010, **195**, 6839.
31 G. A. Becht, J. T. Vaughey and S. J. Hwu, *Chem. Mater.*, 2010, **22**, 1149.
32 H. P. Christian and H. Mullerbuschbaum, *Z. Naturforsch., B: Anorg. Chem., Org. Chem.*, 1975, **30**, 175.
33 M. Eguchi, T. Iwamoto, T. Miura and T. Kishi, *Solid State Ionics*, 1996, **89**, 109.
34 M. Eguchi, A. Komamura, T. Miura and T. Kishi, *Electrochim. Acta*, 1996, **41**, 857.
35 M. Morcrette, P. Rozier, L. Dupont, E. Mugnier, L. Sannier, J. Galy and J. M. Tarascon, *Nat. Mater.*, 2003, **2**, 755.
36 M. Morcrette, P. Martin, P. Rozier, H. Vezin, F. Chevallier, L. Laffont, P. Poizot and J. M. Tarascon, *Chem. Mater.*, 2005, **17**, 418.
37 P. Poizot, F. Chevallier, L. Laffont, M. Morcrette, P. Rozier and J. M. Tarascon, *Electrochem. Solid-State Lett.*, 2005, **8**, A184.
38 L. Zhou, J. Zou, M. M. Yu, P. Lu, J. Wei, Y. Q. Qian, Y. H. Wang and C. Z. Yu, *Cryst. Growth Des.*, 2008, **8**, 3993.
39 L. L. Springsteen and E. Matijevic, *Colloid Polym. Sci.*, 1989, **267**, 1007.
40 L. F. Wang, I. Sondi and E. Matijevic, *J. Colloid Interface Sci.*, 1999, **218**, 545.
41 I. Sondi and E. Matijevic, *J. Colloid Interface Sci.*, 2001, **238**, 208.
42 N. Recham, M. Armand, L. Laffont and J. M. Tarascon, *Electrochem. Solid-State Lett.*, 2009, **12**, A39.
43 G. C. Li, S. P. Pang, L. Jiang, Z. Y. Guo and Z. K. Zhang, *J. Phys. Chem. B*, 2006, **110**, 9383.
44 Y. Wang, H. M. Shang, T. Chou and G. Z. Cao, *J. Phys. Chem. B*, 2005, **109**, 11361.
45 B. Alonso and J. Livage, *J. Solid State Chem.*, 1999, **148**, 16.
46 C. J. Brinker and G. W. Scherer, *Sol Gel Science: the Physics and Chemistry of Sol–Gel Processing*, Academic Press, Inc., New York, 1990, ch. 2, p. 31.
47 J. Livage, *Chem. Mater.*, 1991, **3**, 578.
48 J. M. Song, Y. Z. Lin, H. B. Yao, F. J. Fan, X. G. Li and S. H. Yu, *ACS Nano*, 2009, **3**, 653.
49 X. Y. Cao, J. G. Xie, H. Zhan and Y. H. Zhou, *Mater. Chem. Phys.*, 2006, **98**, 71.
50 P. Rozier, M. Morcrette, P. Martin, L. Laffont and J. M. Tarascon, *Chem. Mater.*, 2005, **17**, 984.